Solar Photocatalytic Degradation of Diclofenac by N-Doped TiO_2 Nanoparticles Synthesized by Ultrasound

Ramandi, Sara; Entezari, Mohammad H.*+; Ghows, Narjes

Sonochemical Research Center, Department of Chemistry, Faculty of Science, Ferdowsi University of Mashhad, Mashhad, I.R. IRAN

ABSTRACT: *Anatase N-doped TiO_2 nanoparticles were synthesized using ultrasound at low frequency and at room temperature. The samples characterized by techniques including XRD, TEM, HRTEM, FT-IR, XPS, and UV–Vis spectroscopy. XPS indicated the existence of nitrogen as an anion dopant within the TiO_2 lattice. The solar photocatalytic activity of N-doped TiO_2 studied for the degradation and complete mineralization of Diclofenac (DCF). The results showed that the catalytic activity of the nanoparticles related to* the *operating conditions in the synthesis such as temperature and time of sonication. DCF degradation followed the pseudo-first-order kinetics model under different conditions. Results showed that photogenerated electrons on the catalyst surface played an important role in the mechanism of photocatalytic degradation of DCF. It also confirmed that in the presence of oxygen, the formation of oxidative species such as singlet oxygen and superoxide radical had major roles in the degradation of DCF.*

KEYWORDS: *Ultrasound; N-doped TiO_2 nanoparticles; Photocatalytic degradation; Diclofenac; Mineralization.*

INTRODUCTION

Anatase titanium dioxide (TiO_2) is a widely used and effective photocatalyst for environmental usages, such as the degradation of organic contaminants, air purification, and antibacterial applications [1, 2]. It is due to its high efficiency, low cost, nontoxicity, and its chemical photostability. However, TiO_2 suffers from its wide band gap (3.2 eV) that can capture only approximately 5% of the total solar irradiation and activated by Ultraviolet Light (UV) [3]. It is necessary to develop photocatalytic activity with visible and solar light [4, 5].

Many endeavors made to vanquish these problems by doping metal and non-metal into the TiO_2 matrix in order to reduce the band gap and improve the visible light photocatalytic activities. But, doping with transition metal ions is thermally unstable and can act as electron–hole recombination sites, which leads to a reduction in the photocatalytic efficiency [6, 7]. It has reported that substitution or interstitial doping of non-metallic elements such as C [8], N [9], S [10], I [11], P [12] can successfully modify the electronic structure of TiO_2 with extending its photoresponse to the visible light region. Among these attempts, doping with nonmetallic ions, especially with the N via anion precursors (amines, nitrates, ammonium salts, ammonia, and urea) [13] has been accepted as the best candidates for doping and extending the optical absorption of TiO_2 into visible light [14, 15]. Some resistant organic

** To whom correspondence should be addressed.*
+ E-mail: entezari@um.ac.ir ; moh_entezari@yahoo.com
1021-9986/2020/3/159-173 15/$/6.05

contaminants degraded under sunlight in recent years [16, 17]. The best candidate of N for doping can be due to its non-poisonous [18], comparable atomic size with oxygen, low ionization energy, metastable center formation, localized energy states formation within titanium band gap, stability, and formation of oxygen vacancies created during the reaction with the anion precursor [19, 20]. The nitrogen doped TiO_2 powder synthesized with the different procedure shown different powder character and different photocatalytic activity due to its crystal structure, the nature and the composition of the dopant that are specified by the preparation methods [18, 20]. Different methods have been used to prepare N-doped photocatalysts, including sputtering techniques [21], solvothermal process [22], sol–gel [23], oxidation of titanium nitride [24], ultrasound [19], and the sol-gel combustion method which has recently brought forth based on the calcination of titania in the presence of urea [25]. However, these methods usually need expensive apparatus [17, 26], require tight control of experimental conditions, and complicated procedures such as annealing at high temperatures under reducing atmospheres [27].

On the other hand, among of environmental pharmaceutical contaminants, great attention has paid on DCF efficient decomposition and mineralization. This is due to its high consumption rate (nearly about 940 tones) and its presence in wastewater that leads to increasing its toxic effect in combination with other drugs present in water [28]. The purpose of this study is to assess the feasibility of the photocatalytic degradation of DCF and mineralization in the presence of TiO_2 and N-doped TiO_2. Therefore, finding novel routes to prepare visible light-responsive TiO_2 is today an important scientific and technological challenge.

In this study, a new sonochemical method planned for the preparation of N-doped TiO_2 nanoparticles under ambient temperature to improve its optical efficiency and catalytic performance under solar light. The synthesis of nanoparticles with ultrasound is easier than other methods for generating novel materials with unusual properties [15, 29] under mild conditions due to the extreme local situation caused by acoustic cavitation (5000 K, 500 bar and cooling rates in excess of 10^9 K/s) [30]. On the other hand, the low-frequency ultrasound could induce morphological, optical and surface changes such as particle association, visible light absorption and oxygen vacancies formation on P-25 TiO_2 nano-particles. This is due to high-speed inter-particle collisions and shock waves which impact on the semiconductor surface and produces surface damage that is responsible for the oxygen vacancy formation [31].

In this paper, we used ultrasonic irradiation in the preparation of N-doped TiO_2 to form a stable anatase phase at ambient temperature. The key point of this work is a short time of sonication in the synthesis process. In addition, the degradation of DCF with complete mineralization in the presence of this photocatalyst has not investigated yet. The new catalyst showed high photocatalytic performance in mineralization of the DCF under sunlight irradiation inside the solution and on the catalyst surface.

EXPERIMENTAL SECTION

Materials

Tetrabutylorthotitanate (purity 98%), n-propanol, urea, potassium persulfate, potassium iodide, 1,4-benzoquinone (BQ), HNO_3, HCl, and NaOH from Merck, NaN_3 from Riedel and diclofenac sodium ($C_{14}H_{10}Cl_2NNaO_2$) from Sigma-Aldrich. All reagents were in analytic grade and used straightly without further purification. Ultrapure Milli-Q water from Millipore used for the preparation of solutions.

Synthesis of N-doped TiO_2

Nanocrystalline N-doped anatase TiO_2 prepared by sonication of the solution of titanium (IV) butoxide and urea. In a typical synthesis, 7.5 mL of tetrabutylorthotitanate added dropwise into 50 mL of MQ water under stirring at room temperature and acidified with 1.5 mL nitric acid. The solution was sonicated at 20 kHz (14.13 W/cm^2) in a Rosset cell at 25^{o}C. The temperature controlled at 25°C through the circulating water. After sonication for 30 min, 15 mL n-propanol added and the translucent colloidal solution became completely transparent. Then, urea (25% w/v) added and for homogenization, the solution sonicated continuously for another 30 min. Subsequently, the resulting transparent nano-sol dried by a first annealing step at 100°C in an oven and further calcined for 2 hours at 450°C for complete crystallization of TiO_2 with a yellowish color. The name of nano-sol used due to the achievement of transparent sol using ultrasound in the sol-gel process [32].

In addition, for comparison, undoped-TiO_2 synthesized with the same procedure without adding urea. The effect of parameters such as temperature, and sonication time investigated in the synthesis process.

Characterization methods

Features synthesized nanoparticles characterized by several techniques. X-ray diffraction (XRD) patterns of all samples were collected in the range of 10^o-80^o using a Bruker-axs, D8 Advance in scanning step of 0.04^0/s, with monochromatic Cu Kα radiation (λ = 1.5406 Å). The superficial morphology and the shape of particles of the samples shown by Transmission electron microscopy (TEM, Philips CM30 300 kV from Netherlands). The X-ray Photoelectron Spectra (XPS) recorded to study the chemical states of the sample with ESCA PHI 5000 instrument (Al Kα irradiation with 1486.6 eV energy and Mg Kα irradiation with 1253.6 eV energy). Fourier Transform InfraRed (FT-IR) spectra recorded with KBr disks comprising the powder sample with the FTIR spectrometer Thermo Nicolet (Avatar 370). UV–Vis spectra of all samples obtained using a UV-Vis spectroscopy (Unico 2800).

Photocatalytic activity measurement

The activities of the as-synthesized samples were estimated by the photocatalytic degradation of DCF solution under sunlight irradiation in summer (GPS co-ordinates: N=36º18'41.6″, E= 59º31' 54.2″). In a typical experiment, 25 mL aqueous suspensions of DCF (25 mg/L) and 1.0 g/L of catalyst added into a water-jacketed reactor. Prior to photocatalytic reaction, the reactor was completely sealed and stirred continuously to reduce the mass transfer limitation and obtaining adsorption/desorption equilibrium between DCF and N-doped TiO_2 for 1 h. At given time intervals, samples withdrawn from the reactor, centrifuged with a speed of 10000 rpm for 10 min and filtered through 0.22 μm Millipore filters to remove N-doped TiO_2 particles for further analysis. Then the supernatant liquid in the photocatalytic reaction analyzed by measuring the maximum absorbance of DCF at 275 nm using the UV-Vis spectrophotometer. The photocatalysis experiments carried out under solar light for 300 min. The initial pH of the solution was unadjusted at pH 6.75, and for the pH studies, it adjusted with either HCl or NaOH. According to photocatalysis experiments, the reactivity of nanoparticles with respect to DCF was investigated as a function of time, pH (1.5~10), loading photocatalyst (0.4~2.8 g/L) and initial concentration of DCF (10~50 mg/L).

The Chemical Oxygen Demand (COD) of samples assessed by dichromate method [33] and it compared with the initial COD of DCF solution [34]. Desorption tests of the DCF from the nano-photocatalyst was carried out by dispersing pre-adsorbed nanocatalyst in 25 mL methanol and stirring continuously with a speed of 300 rpm for 60 min in order to ensure complete desorption. The percent of real degradation calculated using the following formula [15]:

$$\%\,\text{degradation} = \frac{C_0 - [C_t + C_d]}{C_0} \times 100 \qquad (1)$$

Where C_o denotes the initial DCF concentration (mg/L), C_t is the concentration at time t (mg/L) in the solution and C_d is the concentration at time t on the surface of photocatalyst which was measured through the desorption process (mg/L). To determine the main photoinduced reactive species in photocatalytic degradation of DCF by N-doped TiO_2 nanoparticles, the effects of KI (h^+ quencher), $K_2S_2O_8$ (e^- quencher), NaN_3 (O_2^1 quencher), 1, 4-benzoquinone (BQ) ($^{\bullet}O_2^-$ quencher) and Ar-purging and ethanol ($^{\bullet}OH$ quencher) were investigated under sunlight. The same concentration of scavengers (5 mM) used for the solutions of 25 mg/L DCF under optimal conditions.

RESULTS AND DISCUSSION

Characteristics of N-doped TiO_2

XRD analysis

XRD accomplished to investigate the crystal identification of TiO_2 samples and the impact of nitrogen doping on the crystal structure of TiO_2. Fig. 1 shows the XRD patterns of un-doped and N-doped TiO_2 nanoparticles. It shows prominent peaks at angles 2θ = 25.3◦, 37.8◦, 48.0◦, 53.9◦, and 62.7◦, which can be attributed to the (101), (004), (200), (105), and (204) faces of anatase structure of N-doped TiO_2 sample, without other crystal phases (rutile or brookite). It also observed the presence of three phases contained anatase (JCPDS file no. 04-0477), rutile (JCPDS file no. 21-1276) and brookite (JCPDS file no. 03-0380) for the un-doped TiO_2 that anatase phase is maximum according to their peak

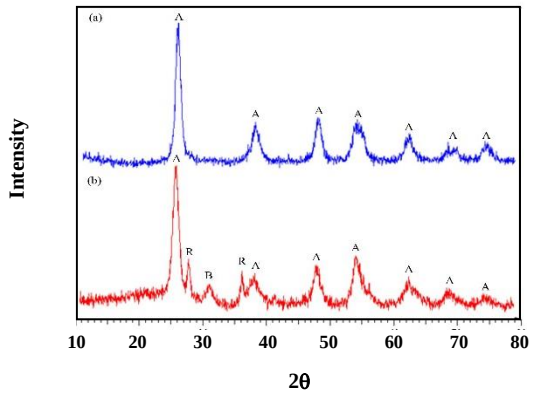

Fig. 1: X-ray diffraction patterns of (a) N-doped TiO_2 and (b) un-doped TiO_2 samples synthesized by ultrasound.

intensities. Commonly, brookite is a transitional phase from anatase to rutile in the heating process. This is due to some of the physical properties of brookite that are between those of anatase and rutile [35]. Thus, it concluded that the addition of N source (urea) favored the formation of anatase and inhibited the formation of rutile. According to the above analysis, we can find out that N-doped TiO_2 nanoparticles should represent considerably high thermal stableness and highly resistant to the phase transformation from anatase to rutile. In addition, no diffraction lines due to TiN observed for the N-doped TiO_2 that this reveals that N anions do not react with TiO_2 to form new crystalline phases such as TiN. In other words, the dopant may have moved into either the interstitial positions or the substitutional sites of the TiO_2 crystal structure [20].

Weight fractions of each phase calculated from the related to integrate characteristic XRD peak intensities according to the quality factor ratio, and the average crystal size was determined from the broadening of the corresponding X-ray spectral peak by the Debye-Scherrer equation [15]:

$$D = \frac{K\lambda}{\beta \cos\theta} \quad (2)$$

Where K is a constant, commonly K=0.89; β is the full-width at half of maximum intensity of the (101) peak; λ is the wavelength of the X-ray CuKα (λ=0.15406 nm) and θ is the Bragg's angle in degree between the incident and diffracted beams. Weight fractions of phases and estimated crystal size of the un-doped and N-doped TiO_2 samples listed in Table 1. The weight percent of anatase in the rutile phase obtained from the following equation [36]:

$$X_A = [1 + 1.26(\frac{I_R}{I_A})] \quad (3)$$

Where X_A is the weight fraction of anatase in the mixture, I_R and I_A obtained from the peak areas of the characteristic anatase (101) and rutile (110) diffraction pattern, respectively. As we known, brookite exhibited no photocatalytic activity, and the band gap of anatase phase was higher than the rutile one. Thus, it induced that N-doped TiO_2 should possess higher photocatalytic activity than that of un-doped TiO_2.

TEM analysis

The morphology of the N-doped TiO_2 sample characterized by TEM, HRTEM, and SAED, as shown in Fig. 2. The sample synthesized under ultrasound showed only anatase phase and no rutile phase detected. The crystallite sizes of the TEM images were consistent with those obtained from XRD spectra. Fig. 2a shows the image of N-doped TiO_2 nanoparticles synthesized by sonication with irregular spherical morphologies with sizes in the range from 8 to 10 nm (average size was estimated with Digimizer software). From the image, the N atoms dispersed into the TiO_2 lattice as dark spots that characterized by XPS technique. Fig. 2b also confirms the average size of the nanoparticles. The SAED pattern shown in Fig. 2c corresponds to the polycrystalline diffraction rings of anatase phase. Surprisingly, no signs of diffraction rings observed related to the other phases.

X-ray Photoelectron Spectroscopy (XPS)

XPS is widely used for the characterization of the surface elemental compound and electronic states of the samples. The XPS measurement of N-doped TiO_2 synthesized by ultrasound shows the existence of four elements: Ti, O, N and C (Fig. 3a). According to the XPS element analysis, the atomic composition of O1s, Ti2p, C1s and N1s are 46.92, 32.80, 17.92 and 2.36%, respectively. The measurements of N1s, C1s, Ti2p and O1s core levels were studied by using this technique. High-resolution Ti2p XPS spectra obtained and demonstrated in Fig 3b. The TiO_2 XPS spectrum was fitted with four peaks (463.8, 464.8, 489 and 470.5 eV). These data are in agreement with previously reported XPS data

Table 1: Phase composition and particle size of TiO_2 samples.

Sample	Phase composition (%)			Particle size (nm)
	Anatase	Rutile	Brookite	
Un-doped TiO_2	76.39	17.60	6.01	8.0
N-doped TiO_2	100	0	0	7.4

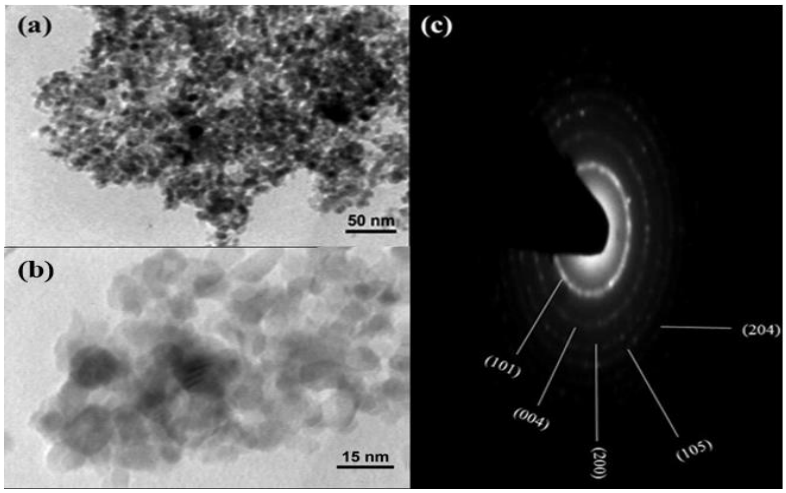

Fig. 2: Images of (a) TEM, (b) HRTEM and (c) SAED pattern of N-doped TiO_2 nanoparticles.

for N-doped TiO_2 [37, 38]. In this study, it is clear that the two different Ti peaks were shifted toward higher binding energy which agrees well with the presence of Ti^{4+} ions in TiO_2 [5]. The O1s XPS spectrum displayed in Fig. 3c deconvoluted as three peaks. The peak at 538.2eV is ascribable to Ti–OH, or C═O, and O–C═O species, and the peaks at 535.1 eV are attributable to oxygen anions in the lattice (Ti–O–Ti). While the peak at 535.6 eV may be appointed to the carbonyl oxygen of O═C–O–Ti bonds or residual –COOH [39]. This is consistent with the result obtained from C1s spectrum. The chemical structure of carbon investigated by the XPS of C1s core levels as shown in the Fig. 3d. Three peaks observed for the C1s at 290.2, 290.8 and 294.3 eV. The first peak observed at 290.2 eV attributed to elemental carbon present on the surface, which is consistent with previous studies. The absence of C1s peak at 281 eV, characteristic of Ti-C bonds, indicates that carbon cannot doped into the TiO_2 lattice [40]. The second and third peaks at 290.8, 294.3 eV are ascribed to C-O and C=O bonds, respectively [41], which indicates the formation of carbonated species [42]. The N1s XPS spectra for N-doped TiO_2 shown in Fig. 3e, the wide peak can fitted by two peaks at 411.6 and 404.7 eV. The peak with a binding energy of around 404.7 eV attributed to the substitution of N in the form of O–Ti–N. This confirms that partial of the O atom in the lattice of TiO_2 was substituted by N^- anions. The N1s peak at 411.6 eV ascribed to the interstitial N-doping or the formation of Ti–O–N species. In fact, when the N atom substituted by O atom in the lattice of TiO_2 led to decreasing electron density around N due to the further electro-negativity of the O atom, resulted in the shift of binding energies [43].

FT-IR analysis

Fig. 4 shows the FT-IR spectra of the N-doped and un-doped TiO_2 prepared by ultrasound approach. The peak at 925 cm^{-1} is attributed to the stretching vibration of O-Ti-O that after adding urea it has shifted to lower frequencies

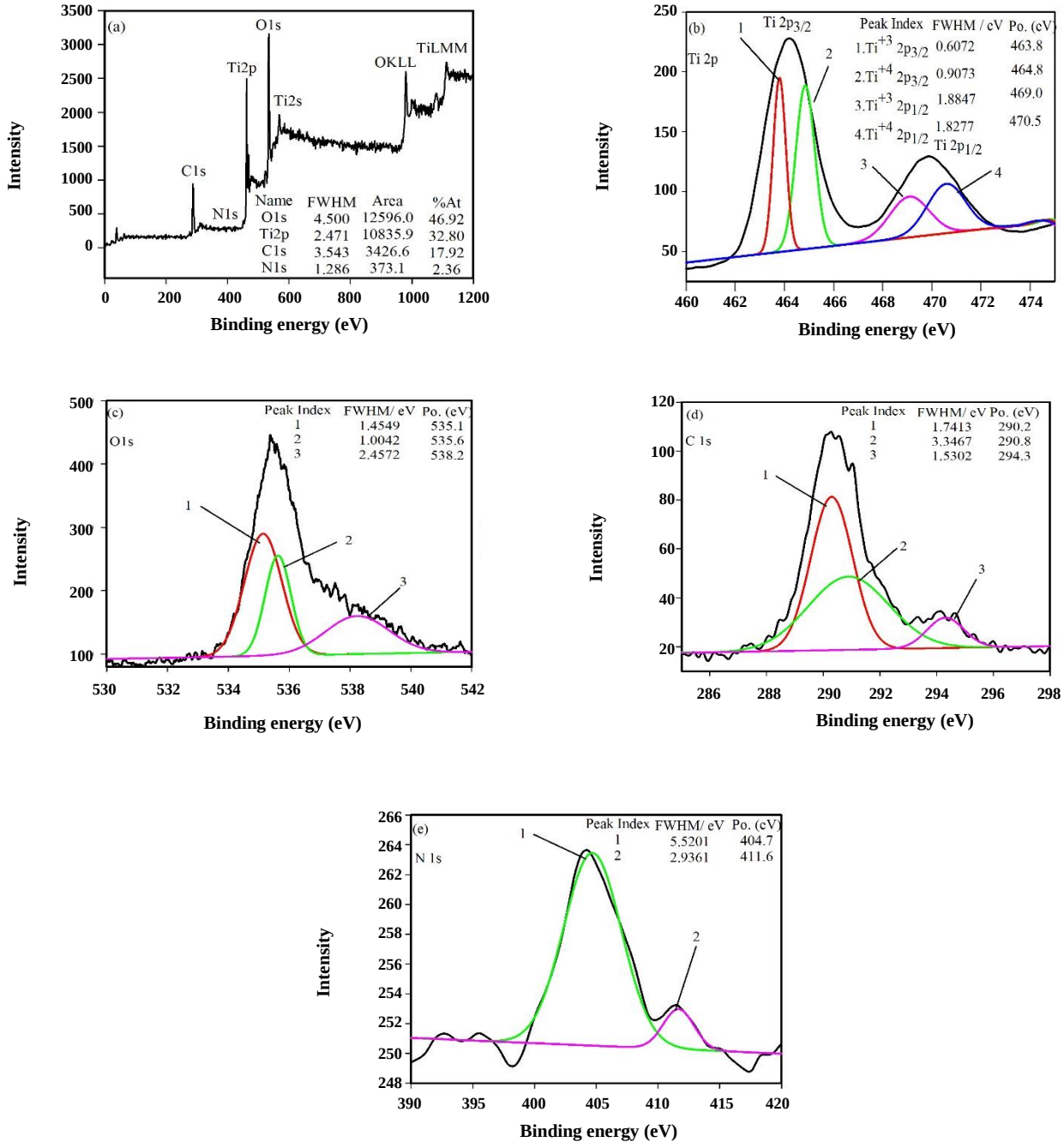

Fig. 3: (a) XPS survey spectrum and high-resolution XPS scan spectra of (b) Ti2p, (c) O1s, (d) C1s and (e) N1s of N-doped TiO_2.

as observed at around 750.46 cm^{-1} [44], which might cause due to the O-Ti-N structure. The broad bands at 2600-3600 cm^{-1} are devoted to the O-H vibration for water molecules and Ti-OH and the peak at around 1620-1630 cm^{-1} can assigned to bending vibrations of O–H [45]. The peak around 2050 cm^{-1} of N-doped TiO_2 sample can be attributed to the presence of C=N, C=C and C=O conjugated bonds of persistent organic species that coordinate with TiO_2 via oxygen surface atoms. This can be responsible for the visible-light-active response of the doped materials [46]. The peak at around 1440.36 cm^{-1} assigned to the vibrations of the Ti–N [38]. The

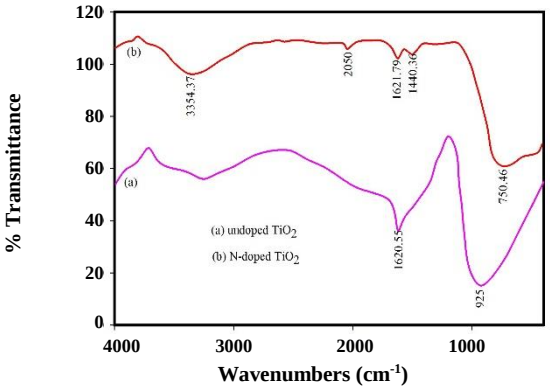

Fig. 4: FT-IR spectra of un-doped and N-doped TiO_2 nanoparticles.

appearance of this peak proposes that the N species have incorporated into the TiO_2 lattice.

UV-Vis spectroscopy

Fig. 5a shows the UV–Vis absorption spectra of the N-doped and un-doped TiO_2. The un-doped sample displayed an absorption edge at 375 nm for TiO_2, while doping sample represented a red shift in the absorption edge toward the visible light region, which is consistent with the changes in the color of the sample from white to yellowish. In fact, nitrogen can represent an impurity level between the valence and conduction band of TiO_2 [47] or narrow the band gap by mixing the N (2p) and O (2p) states [17] that lead to the shift of absorption in the visible range. The band gap energies can evaluated from the absorption spectra. Semiconductors are categorized to be directly or indirect pursuant to the lowest permissible electronic transition. The band gap energies calculated according to the Tauc equation (Eq. (4)) [15]:

$$(\alpha h\nu)^{\frac{1}{n}} = A(h\nu - E_g) \quad (4)$$

Where *h*: Planck's constant, *v*: frequency of vibration, α: absorption coefficient, E_g: band gap and A: proportional constant. The value of the exponent *n* indicates the nature of the sample transition: for direct allowed transition (n =1/2), for direct prohibited transition (n = 3/2), for indirect allowed transition (n = 2) and for indirect forbidden transition (n = 3) [48] that the value of N-doped TiO_2 is equal to 2. A plot of $(\alpha hv)^{1/2}$ versus E_g affords the band gap energy with extrapolating the linear part of the corresponding curves as shown in Fig. 5b. The obtained band gap values were 3.2 and 2.7 eV for un-doped TiO_2 and N-doped TiO_2, respectively.

DCF degradation by N-doped TiO_2

Effect of temperature on the synthesis of N-doped TiO_2

Temperature is an important variable in the synthesis of nanoparticles. Samples were prepared at 25, 40 and 80°C under optimized conditions to study the influence of temperature on the degradation of DCF. Fig. 6 presents the effect of different temperatures for the preparation of N-doped TiO_2 in the degradation of DCF under sunlight within 3 hours. The synthesized nanophotocatalyst by ultrasound (20 kHz) at 25°C exhibited the highest activity in the mineralization of DCF. On the other hand, the sample prepared at the highest temperature (80°C) in comparison with low temperatures showed the lowest efficiency and this is due to the decrease of the critical conditions produced during the cavitation at the highest temperature [15]. Hence, the synthesized nanophotocatalyst by ultrasound (20 kHz) at 25°C selected for other experiments.

Effect of sonication time on the synthesis of N-doped TiO_2

Fig. 7 shows the photocatalytic activity of the various samples with different sonication time. When the sonication time increased from 30 min to 60 min, an increase in the degradation of DCF observed. This attributed to the fact that as the sonication time is increased, the overall cavitation effects in the system increase too. However, by increasing the time of sonication, beyond 60 min, the N-doped TiO_2 showed a lower photocatalytic activity. This may be dependent on the effect of ultrasound on the crystal structure at the longer sonication time [15].

Effect of other important variables on the degradation of DCF

Further experiments under different process conditions such as catalyst dosage, the initial concentration of DCF, solution pH, and reaction temperature performed and the results summarized in Table 2. The results disclose that the photocatalytic degradation of DCF under different operation conditions followed a pseudo-first-order kinetics model.

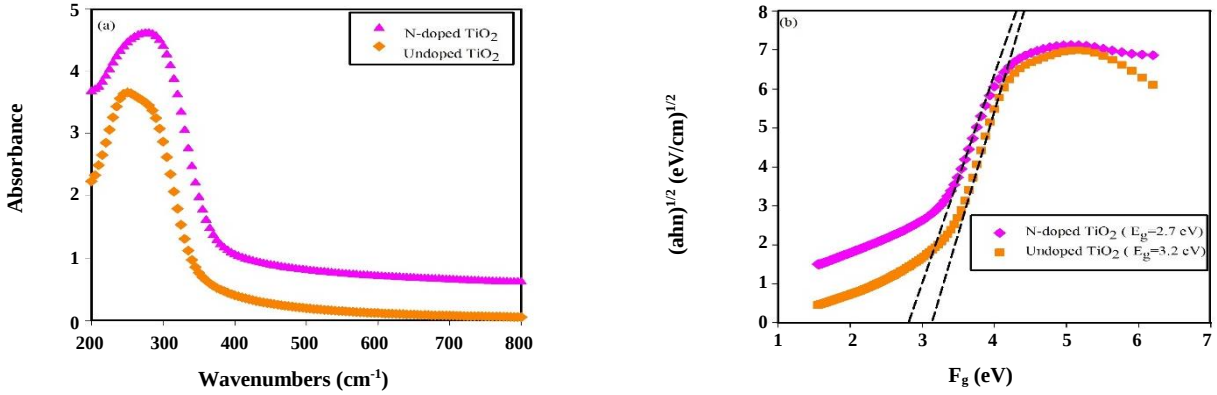

Fig. 5: (a) UV-Vis absorption spectra and (b) plots of $(\alpha h\nu)^{1/2}$ versus E_g of un-doped and N-doped TiO_2.

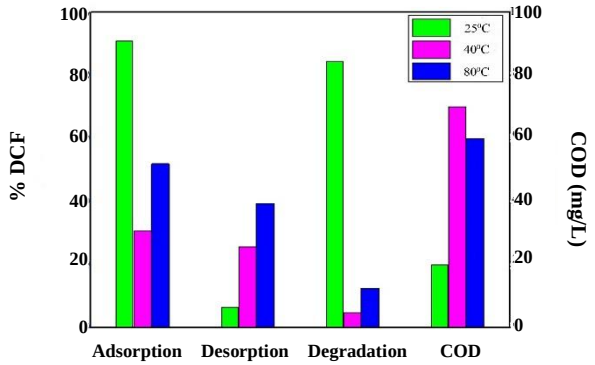

Fig. 6: N-doped TiO_2 nanoparticles prepared at different temperatures for the degradation of DCF under solar light (C_0 : 25 mg/L, 1.0 g/L catalyst, pH 6.7, 25°C, time, 3 hours).

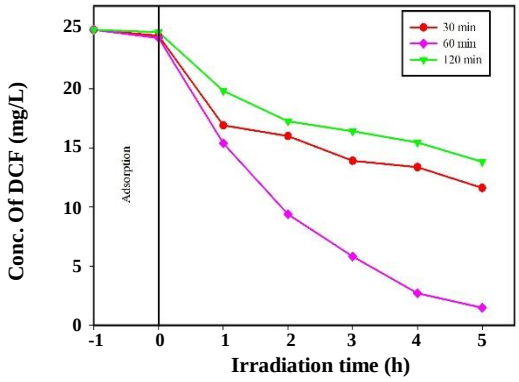

Fig. 7: Degradation of DCF under sunlight by N-doped TiO_2 synthesized at different times of sonication (25 mg/L DCF, 1.0 g/L catalyst, pH 6.7, 25°C).

The Langmuir–Hinshelwood (L-H) kinetic model considered for the photocatalytic degradation of DCF (Eq. 5) [15]:

$$r_0 = -\frac{dC}{dt} = \frac{k_r K C_0}{1 + K C_0} \quad (5)$$

Where r_0 is the initial reaction rate (mg / L.min), C_0 is the initial concentration of DCF (mg/L), t is the reaction time (min), k_r is the Langmuir-Hinshelwood reaction rate constant (mg/L.min), and K is the adsorption equilibrium constant (L/mg). When the amount of adsorption and/or substrate concentration is low (KC<< 1) Eq. (5) reduced to a first-order kinetic model according to the Eq. 6:

$$-\frac{dC}{dt} = k_a C \Leftrightarrow \ln\frac{C}{C_0} = -k_a t \quad (6)$$

Where k_a the apparent rate constant (min^{-1}) and C_0 is the initial concentration of DCF (mg/L). The rate constant calculated from the linearity of the plots of $\ln\frac{C}{C_0}$ versus contact time at different concentration (Eq. 6). According to the data, r_0 can be calculated from k_a and C_0 ($r_0 = k_a C_0$, mg/L.min).

Photocatalytic mineralization of DCF under sunlight irradiation

Fig. 8a shows the UV-Vis spectra of DCF solution before and after sunlight irradiation at different interval times. Fig. 8b shows the adsorption, desorption, degradation and COD of the DCF solution versus time in the presence of N-doped TiO_2 under solar light irradiation. The characteristic absorption peak of DCF solution

Table 2: Results of batch experiments for degradation of DCF by N-doped TiO_2 photocatalyst.

Photocatalyst	N-TiO_2(g/L)	C_0(mg/L)	pH	Temperature (^{0}C)	k_a(min^{-1})	r_0 (mg / L min)	$t_{1/2}$ (min)	R^2
1. Effect of photocatalyst type								
Photolysis	-	25	6.7	25	0.0004	0.0100	1732.8	0.9882
TiO_2 (20kHz)	1.0	25	6.7	25	0.0005	0.0125	1380.0	0.9917
N-TiO_2 (20kHz)	1.0	25	6.7	25	0.0091	0.2275	75.8	0.9922
N-TiO_2 (classic)	1.0	25	6.7	25	0.0034	0.0850	202.9	0.9847
2. Effect of photocatalyst loading								
N-TiO_2 (20kHz)	0.4	25	6.7	25	0.0056	0.1400	123.2	0.9880
	0.6	25	6.7	25	0.0082	0.2050	84.1	0.9909
	1.0	25	6.7	25	0.0091	0.2275	75.8	0.9922
	1.2	25	6.7	25	0.0085	0.2125	81.1	0.9908
	2	25	6.7	25	0.0072	0.1800	95.8	0.9926
	2.8	25	6.7	25	0.0067	0.1675	102.9	0.9644
3. Effect of solution pH								
N-TiO_2 (20kHz)	1.0	25	1.5	25	0.0079	0.1975	87.3	0.9940
	1.0	25	2.5	25	0.0056	0.1400	123.2	0.9914
	1.0	25	3.5	25	0.0035	0.0875	197.1	0.9904
	1.0	25	6.7	25	0.0091	0.2275	75.8	0.9922
	1.0	25	10.0	25	0.0016	0.0400	431.2	0.9937
4. Effect of initial DCF concentration								
N-TiO_2 (20kHz)	1.0	10	6.7	40	0.0188	0.4700	36.7	0.9996
	1.0	25	6.7	40	0.0121	0.3025	57.0	0.9943
	1.0	50	6.7	40	0.0063	0.1575	109.5	0.9882

at 275 nm was remarkable decreased in intensity with increasing the irradiation time. The intensity of the peak approaches to zero and no new absorption peaks was appearing in this region, indicating the solution has been completely degraded. The results of the desorption show that the adsorbed DCF remaining on the surface was very low in comparison with the adsorption and confirmed that the adsorption and degradation of the DCF are carried out simultaneously on the catalyst surface. The photocatalytic mineralization of DCF followed by measuring the COD during the process (Fig. 8b). When the DCF on the photocatalyst surface converted to inorganic species under solar radiation, the DCF in solution displaced. The light oxidation continues until the total adsorbed DCF converted to the mineral species [49].

Reusability of N-doped TiO_2 photocatalyst

Fig. 9 shows the percent of DCF degradation by the recoverable N-TiO_2 nanophotocatalyst in four consecutive cycles without changing and significant loss in activity. After each cycle, nanoparticles filtered, washed completely with water, dried and a fresh solution of DCF added for photocatalytic reaction. All experiments conducted with 1.0 g/L of nanocatalyst at 40^{o}C for 5 h under solar light.

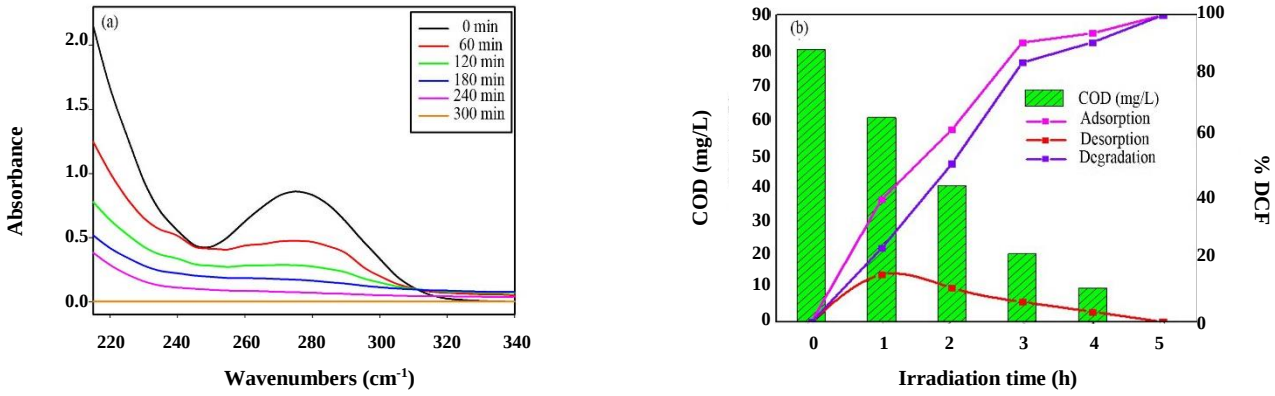

Fig. 8: a) UV-Vis absorption spectra of DCF at different interval times in the presence of N-doped TiO_2 photocatalyst, (b) adsorption, desorption, degradation and COD of the DCF versus time in the presence N-doped TiO_2 under solar light irradiation (C_0 : 25 ppm, 1.0 g/L catalyst, pH: 6.7, 40^0C).

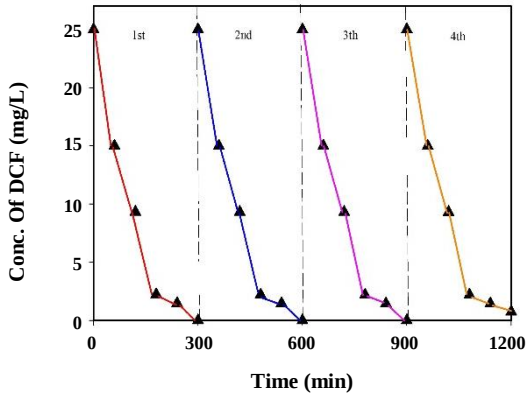

Fig. 9: Reusable of N-doped TiO_2 for photocatalytic degradation of DCF.

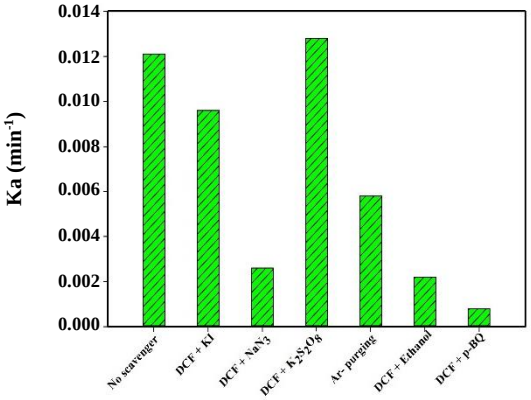

Fig. 10: Rate constants degradation of DCF in the presence of scavengers.

Photocatalytic mechanism of N-doped TiO_2 under sunlight irradiation

The transference of electrons in the photocatalytic process is very important and leads to increase the activity through inhibiting the recombination of electrons and holes on the catalyst surface. Hence, to investigate the mechanism of degradation, scavengers for electrons and holes were employed to determine the photoinduced reactive species such as e^-, h^+, $^{\bullet}OH$, $O_2^{\bullet-}$, and $^1O_2$ that have been suggested to play important roles in the photo-degradation process [38, 50]. In this study, ethanol as a scavenger of $HO^{\bullet}$, potassium iodide (KI) as a scavenger of both h_{vb}^+ and $HO^{\bullet}$, sodium azide (NaN_3) as a $^1O_2$ quencher, potassium persulfate ($K_2S_2O_8$) as an electron acceptor, 1,4-benzoquinone as an $O_2^{\bullet}$ quencher and Ar atmosphere were used. The inhibitory effect of the applied scavengers has been expressed as the percent reduction of kinetic constants (% Δk, Table 3). The degradation kinetics of DCF in the presence of various scavengers demonstrated in Fig. 10, and the variation of pseudo-first-order rate constants summarized in Table 3.

KI is a scavenger and reacts with h_{vb}^+ [51], reducing the number of oxidizing species available at the surface of the catalyst for the reaction with DCF. When 5 mM KI was used as a quencher for stopping the hole process, the decomposition rate constant of DCF was slightly decreased to 0.0096 min^{-1}. This result indicates that the holes were not the active oxidative species involved directly in the photodegradation process of DCF under sunlight.

In order to investigate whether the photocatalytic degradation of DCF takes place via $^{\bullet}OH$, 5 mM ethanol

Table 3: Kinetics parameters of photocatalytic degradation in the presence of scavengers. The inhibitory effect of the applied scavengers has been expressed as the percent reduction of kinetic constants (% Δk).

	Scavengers	RSs quenched	k_a (min^{-1})	$t_{1/2}$ (min)	% Δk
	Control (no scavenger)		0.0121	57.02	
	KI	h_{vb}^+	0.0096	71.87	20.66
	NaN_3	$^1O_2$	0.0026	265.38	78.51
Diclofenac	Ethanol	$^{\bullet}OH$	0.0022	213.63	81.81
	$K_2S_2O_8$	e_{CB}^-	0.0128	53.90	
	Ar-purging	H_2O_2/ $^{\bullet}O_2^-$	0.0058	118.96	52.06
	p-Benzoquinone	$^{\bullet}O_2^-$	0.0008	862.50	93.38

was added to the suspension. The results presented that ethanol significantly inhibited the photocatalytic degradation of DCF under sunlight irradiation for 5 h with rate constant 0.0022 min^{-1}. From this experiment**,** it concluded that $^{\bullet}OH$ radicals play a very important role in the degradation of DCF in the presence photocatalyst under the simulated sunlight irradiation.

Sodium azide (NaN_3) has applied as singlet oxygen ($^1O_2$) quencher. N_3^- is very reactive towards $^1O_2$ (rate constant of this reaction is 2×10^9 $M^{-1}s^{-1}$) with the formation of azidyl radical ($N_3^{\bullet}$) and the superoxide radical anion [52]. Here, in the presence of sodium azide, the DCF degradation rate constant significantly decreased to 0.0026 min^{-1}, suggesting the occurrence of singlet oxygen in the degradation.

P-benzoquinone (p-BQ) is the scavenger of the superoxide radical [53] and its rate constant value with $O_2^{\bullet-}$ is $0.9\text{-}1\times10^9$ M^{-1} S^{-1} [52]. As observed, p-BQ seems to have a negative influence on the degradation of the DCF, which could suggest the participation of $O_2^{\bullet-}$ on the process and confirmed that the superoxide radicals were the major reactive species in the photocatalytic reaction system for photocatalyst.

Dissolved O_2 as an efficient electron scavenger excluded by Ar-purging (saturated condition) in the degradation process. As shown in Table 3, the amount of DCF removal obviously reduced by Ar-purging with the rate constant of 0.0058 min^{-1} in analogy with the case of air equilibrium. The result illustrated that the dissolved oxygen acted as an acceptor of photogenerated e^- in heterogeneous photocatalysis, which led to postponing the recombination of photogenerated e^- and h^+ through the formation of reactive species.

To investigate the role of the photogenerated electron, potassium persulfate ($K_2S_2O_8$) used as a more efficient electron acceptor. This scavenger increased DCF decomposition rate and confirmed that reaction mechanism was via electrons. Reaction mechanism in the presence of potassium persulfate expressed by Equation (7) [54]:

$$S_2O_8^{-2} + e_{CB}^- \rightarrow SO_4^{-\bullet} + SO_4^{-2} \quad (7)$$

The $SO_4^{-\bullet}$ can participate in the DCF decomposition by direct reaction with target molecules. These radicals may also react with generated photoelectrons and the water molecules to produce hydroxyl radicals according to Equations (8) and (9):

$$SO_4^{-\bullet} + e_{CB}^- \rightarrow SO_4^{-2} \quad (8)$$

$$SO_4^{-\bullet} + H_2O \rightarrow HO^{\bullet} + SO_4^{-2} + H^+ \quad (9)$$

On basis of the above experimental results, the transfer of electrons further confirmed to be responsible for the degradation and the active species generated by electrons such as singlet oxygen and superoxide radicals were the major responsibility in the degradation of DCF.

The formation of defects into the TiO_2 anatase lattice improves the electronic band structure of TiO_2 that leads to the narrowing of the band gap of TiO_2 and the creation of oxygen vacancy acts as the color center, which both of them enhances visible light absorbance. In addition, the excess photo-induced electrons departed from the oxygen vacancies can cause reduction of the Ti^{4+} and the generation of Ti^{3+} color center. This reduction is accompanied by the formation of the 3d orbital of the Ti^{3+}

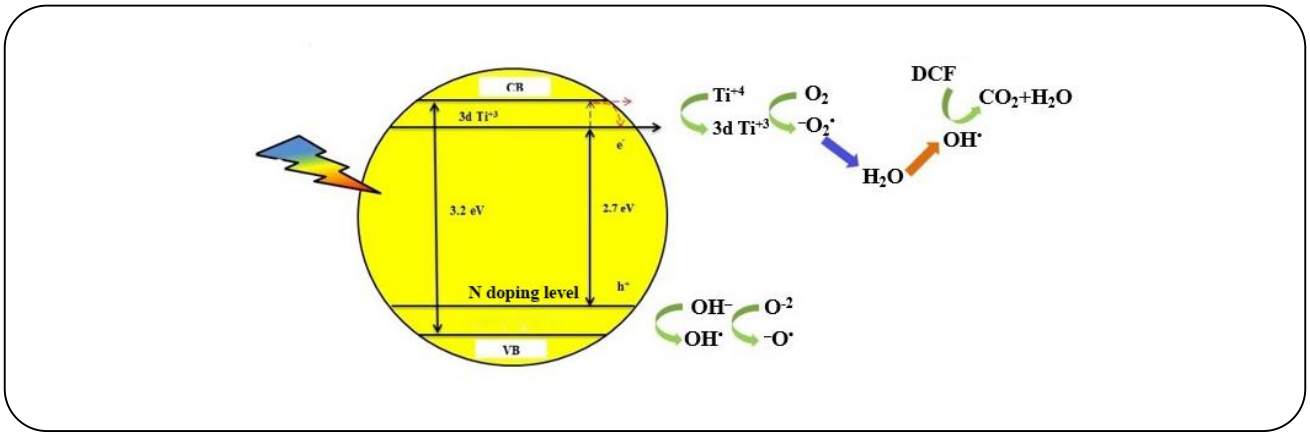

Fig. 11: Schematic illustration of the charge separation and transfer process in N-doped TiO_2 for the degradation of DCF under sunlight irradiation.

ions in the band gap and contributes to the visible light absorption in N-doped TiO_2 [38]. On basis of the above experimental results and the electronic band structure of TiO_2, a possible mechanism for the solar light degradation of DCF over the N-doped TiO_2 proposed (Fig. 11). As shown in Fig. 11, under solar light irradiation, the electrons transfer directly into the conduction band of TiO_2 and reduce the adsorbed O_2 to form active species responsible for the degradation of DCF.

On the other hand, as it was stated the photocatalytic performance of the N-doped TiO_2 semiconductor related to many important parameters such as oxygen vacancies, Ti^{3+} color center, band gap, particle size, surface area, kind of phases, and crystallinity. These parameters strongly depend on the kind of method that the N-doped TiO_2 is prepared and its preparation temperature [5, 20]. This study clearly demonstrates the importance of ultrasound in the photocatalytic performance of N-doped TiO_2.

CONCLUSIONS

In summary, a new method has applied for the synthesis of N-doped TiO_2 nanoparticles by low-frequency ultrasound (20 kHz) at 25ºC in order to increase the photocatalytic efficiency and complete mineralization of the DCF under solar light. This study clearly demonstrates the importance of ultrasound in the improvement of the photocatalytic performance of N-doped TiO_2. The crystalline phase of N-doped TiO_2 in the presence of ultrasound was only the anatase phase while other phases observed in other samples. Furthermore, achieving a nanophotocatalyst with maximum optical absorption in the visible range and complete mineralization of DCF under solar light attributed to the harsh conditions produced during the cavitation process. The degradation of DCF conducted under different variables and the perfect mineralization obtained in 5 h. In addition, the degradation fitted to the first-order kinetics model. The excellent photocatalytic performance was due to the formation of oxidative species such as singlet oxygen and superoxide radical by electrons on the catalyst surface. The simplicity of the process, preparation at low temperature by low-frequency ultrasound, and complete mineralization in ambient conditions considered as the advantages of this method.

Acknowledgment

The authors acknowledge the help given by Mr. Daliyani from Solid State Physics Research Center, Damghan University. The support of Ferdowsi University of Mashhad (Research and Technology) is appreciated for the project (3/20243, 17/12/2011). The authors also acknowledge the support of the 'Iranian National Science Foundation: INSF (No. 92040178)' for this work.

Received : Aug. 2, 2018 ; Accepted :Jan. 28, 2019

REFERENCES

[1] Zatloukalová K., Obalová L., Kočí K., Čapek L., Matěj Z., Šnajdhaufová H., Ryczkowski J., Słowik G., Photocatalytic Degradation of Endocrine Disruptor Compounds in Water over Immobilized TiO_2 Photocatalysts, *Iran. J. Chem. Chem. Eng. (IJCCE)*, **36**: 29-38 (2017).

[2] Fagan R., Synnott D.W., McCormack D.E., Pillai S.C., An Effective Method for the Preparation of High Temperature Stable Anatase TiO_2 Photocatalysts, *Appl. Sur. Sci.*, **371**: 447-452 (2016).

[3] Xie M., Feng Y., Luan Y., Fu X., Jing L., Facile Synthesis of N-doped TiO_2 and Its Enhanced Photocatalytic Activity for Degrading Colorless Pollutants, *Chem. Plus. Chem.*, **79**(5): 737-742 (2014).

[4] Yoshida T., Niimi S., Yamamoto M., Nomoto T., Yagi S., Effective Nitrogen Doping into TiO_2 (N-TiO_2) for Visible Light Response Photocatalysis, *J. Colloid Interface Sci.*, **447**: 278-281 (2015).

[5] Bahramian A. R., Enhanced Photocatalytic Activity of Sol-Gel Derived Coral-Like TiO_2 Nanostructured Thin Film, *Iran. J. Chem. Chem. Eng. (IJCCE)*, **35**(2): 27-41 (2015).

[6] Shogh S., Mohammadpour R., Iraji zad A., Taghavinia N., A New Sterategy on Utilizing Nitrogen Doped TiO_2 in Nanostructured Solar Cells: Embedded Multifunctional N-TiO_2 Scattering Particles in Mesoporous Photoanode, *Mater. Res. Bull.*, **72**: 64-69 (2015).

[7] Ananpattarachai J., Seraphin S., Kajitvichyanukul P., Formation of Hydroxyl Radicals and Kinetic Study of 2-Chlorophenol Photocatalytic Oxidation Using C-doped TiO_2, N-doped TiO_2, C, N Co-Doped TiO_2 Under Visible Light, *Environ. Sci. Poll. Res.*, **23**(4): 3884-3896 (2016).

[8] Lin Y. T., Weng C. H., Chen F. Y., Key Operating Parameters Affecting Photocatalytic Activity of Visible-Light-Induced C-Doped TiO_2 Catalyst for Ethylene Oxidation, *Chem. Eng. J.*, **248**: 175-183 (2014).

[9] Fan J., Zhao Z., Liu W., Xue Y., Yin S., Solvothermal Synthesis of Different Phase N-TiO_2 and Their Kinetics, Isotherm and Thermodynamic Studies on the Adsorption of Methyl Orange, *J. Colloid and Interface Sci.*, **470**: 229-236 (2016).

[10] Ni J., Fu S., Wu C., Maier J., Yu Y., Li L., Self-Supported Nanotube Arrays of Sulfur-doped TiO_2 Enabling Ultrastable and Robust Sodium Storage, *Adv. Mater.*, **28**(11): 2259-2265 (2016).

[11] Kuo C. Y., Hsiao H. M., Preparation of Iodine Doped Titanium Dioxide to Photodegrade Aqueous Bisphenol A under Visible Light, *Process Safety Environ. Protec.*, **95**: 265-270 (2015).

[12] Xia Y., Jiang Y., Li F., Xia M., Xue M., Li Y., Effect of Calcined Atmosphere on the Photocatalytic Activity of P-Doped TiO_2, *Appl. Surf. Sci.*, **289**: 306-315 (2014).

[13] Jyothi M. S., Souza Laveena P. D., Shewetharani R., Balakrishna G. R., Novel Hydrothermal Method for Effective Doping of N and F into Nano Titania for Both, Energy and Environmental Applications, *Mater. Res. Bull.*, **74**: 478-484 (2016).

[14] Li H., Hao Y., Lu H., Liang L., Wang Y., Qiu J., Shi X., Wang Y., Yao J., A Systematic Study on Visible-Light N-doped TiO_2 Photocatalyst Obtained from Ethylenediamine by Sol-Gel Method, *Appl. Surf. Sci.*, **344**: 112-118 (2015).

[15] Ramandi S., Entezari M. H., Ghows N., Sono-Synthesis of Solar Light Responsive S–N–C–tri Doped TiO_2 Photo-catalyst under Optimized Conditions for Degradation and Mineralization of Diclofenac, *Ultrason. Sonochem.*, **38**: 234-245 (2017).

[16] Zhou X., Lu J., Jiang J., Li X., Lu M., Yuan G., Wang Z., Zheng M., Seo H. J., Simple Fabrication of N-Doped Mesoporous TiO_2 Nanorods with the Enhanced Visible Light Photocatalytic Activity, *Nanoscale Res. Lett.*, **9**: 34-40 (2014).

[17] Vaiano V., Sacco O., Lervonilo G., Sannino D., Ciambelli P., Rigouri R., Bezzeccheri E., Rubino A., Enhanced Visible Light Photocatalytic Activity by Up-Conversion Phosphors Modified N-Doped TiO_2, *Appl. Catal. B: Environ.*, **176-177**: 594-600 (2015).

[18] Mamane H., Horovitz I., Lozzi L., Di Camilo D., Avisar D., The Role of Physical and Operational Parameters in Photocatalysis by N-Doped TiO_2 Sol-Gel Thin Films, *Chem. Eng. J.*, **257**: 159-169 (2014).

[19] Selvaraj A., Sivakumar S., Ramasamy A. K., Balasubramanian V., Photocatalytic Degradation of Triazine Dyes over N-Doped TiO_2 in Solar Radiation, *Res. Chem. Intermediates*, **39**(6): 2287-2302 (2013).

[20] Gurkan Y. Y., Turkten N., Hatipoglu A., Cinar Z., Photocatalytic Degradation of Cefazolin over N-Doped TiO_2 under UV and Sunlight Irradiation: Prediction of the Reaction Paths *via* Conceptual DFT, *Chem. Eng. J.*, **184**: 113-124 (2012).

[21] Powell M. J., Dunnill C. W., Parkin I. P., N-Doped TiO_2 Visible Light Photocatalyst Films *via* a Sol-Gel Route Using TMEDA as the Nitrogen Source, *J. Photochem. Photobio. A: Chem.*, **281**: 27-34 (2014).

[22] Sabri N. A., Nawi M. A., Nawawi W. I., Porous Immobilized C Coated N-Doped TiO_2 Containing In-Situ Generated Polyenes for Enhanced Visible Light Photocatalytic Activity, *Optical Mater.*, **48**: 258-266 (2015).

[23] Liu W. X., Jiang P., Shao W. N., Zhang J., Cao W. B., A Novel Approach for the Synthesis of Visible-Light-Active Nanocrystalline N-Doped TiO_2 Photocatalytic Hydrosol, *Solid State Sci.*, **33**: 45-48 (2014).

[24] Larumbe S., Monge M., Gomez-Polo C., Comparative Study of (N, Fe) Doped TiO_2 Photocatalysts, *Appl. Surf. Sci.*, **327**: 490-497 (2015).

[25] Ghugal S. G., Umare S. S., Sasikala R., Enhanced Photocatalytic Activity of TiO_2 Assisted by Nb, N and S Multidopants, *Mater. Res. Bull.*, **61**: 298-305 (2015).

[26] Liu H., Yao T., Ding W., Wang H., Ju D., Chai W., Study on the Optical Property and Surface Morphology of N-Doped TiO_2 Film Deposited with Different N_2 Flow Rates by DCPMS, *J. Environ. Sci.*, **25**: 54-58 (2013).

[27] Zhao W., Li Y., Zhang M., Chen J., Xie L., Shi Q., Zhu X., Direct Microwave-Hydrothermal Synthesis of Fe-Doped Titania with Extended Visible-Light Response and Enhanced H_2-Production Performance, *Chem. Eng. J.*, **283**: 105-113 (2016).

[28] Martínez C., Canle M. L., Fernández M. I., Santaballa J. A., Faria J., Aqueous Degradation of Diclofenac by Heterogeneous Photocatalysis Using Nanostructured Materials, *Appl. Catal. B: Environ.*, **107**(1-2): 110-118 (2011).

[29] Maleki M., Haghighi M., Sono-Dispersion of CuS-CdS over TiO_2 in One-Pot Hydrothermal Reactor as Visible-Light-Driven Nanostructured Photocatalyst, *J. Mole. Catal. A: Chem.*, **424**: 283-296 (2016).

[30] Chaudhary R. P., Koymen A. R., Synthesis of Magnetic GdC_2 Nanoparticles Using Cavitation Plasma, *Mater. Lett.*, **158**: 194-197 (2015).

[31] Osorio-Vargas P. A., Pulgarin C., Sienkiewicz A., Pizzio L. R., Blanco M. N., Torres-Palma R. A., Pétrier C., Rengifo-Herrera J. A., Low-Frequency Ultrasound Induces Oxygen Vacancies Formation and Visible Light Absorption in TiO_2 P-25 Nanoparticles, *Ultrason. Sonochem.*, **19**(3): 383-386 (2012).

[32] Lee Y.G., Park J.H., Oh C., Oh S.G., Kim Y.G., Preparation of Highly Monodispersed Hybrid Silica Spheres Using a One-Step Sol-Gel Reaction in Aqueous Solution, *Langmuir*, **23** (22): 10875–10878 (2007).

[33] Bartram J., Balance R., "Water Quality Monitoring: A Practical Guide to the Design and Implementation of Freshwater Quality Studies and Monitoring Programmes", *World Health Organization*, London (1996).

[34] Ziylan A., Koltypin Y., Gedanken A., Ince N. H., More on Sonolytic and Sonocatalytic Decomposition of Diclofenac Using Zero-Valent Iron, *Ultrason. Sonochem.*, **20**(1): 580-586 (2013).

[35] Li J.G., Ishigaki T., Sun X., Anatase, Brookite, and Rutile Nanocrystals *via* Redox Reactions under Mild Hydrothermal Conditions: Phase-Selective Synthesis and Physicochemical Properties, *J. Phys. Chem. C*, **111** (13): 4969-4976 (2007).

[36] Prasad K., Pinjari D. V., Pandit A. B., Mhaske S. T., Phase Transformation of Nanostructured Titanium Dioxide from Anatase-to-Rutile *via* Combined Ultrasound Assisted Sol-Gel Technique, *Ultrason. Sonochem.*, **17**(2): 409-415 (2010).

[37] Davis Z. D., Tatarchuk B. J., Understanding the Dispersion of Ag on High Surface Area TiO_2 Supports Using XPS Intensity Ratios, *Appl. Surf. Sci.*, **353**: 679-685 (2015).

[38] Daghrir R., Drogui P., Delegan N., El Khakani M. A., Electrochemical Degradation of Chlortetracycline Using N-Doped Ti/TiO_2 Photoanode Under Sunlight Irradiations, *Water Res.*, **47**(17): 6801-6810 (2013).

[39] Janitabar Darzi S., Movahedi M., Visible Light Photodegradation of Phenol Using Nanoscale TiO_2 and ZnO Impregnated with Merbromin Dye: A Mechanistic Investigation, *Iran. J. Chem. Chem. Eng. (IJCCE)*, **33**(2): 55-64 (2014).

[40] Liu C., Zhang L., Liu R., Gao Z., Yang X., Tu Z., Yang F., Ye Z., Cui L., Xu C., Li Y., Hydrothermal Synthesis of N-doped TiO_2 Nanowires and N-doped Graphene Heterostructures with Enhanced Photocatalytic Properties, *J. Alloys Compd.*, **656**: 24-32 (2016).

[41] Strzemiecka B., Voelkel A., Donate-Robles J., Martin-Martinez J. M., Assessment of the Surface Chemistry of Carbon Blacks by TGA-MS, XPS and Inverse Gas Chromatography Using Statistical Chemometric Analysis, *Appl. Surf. Sci.*, **316**: 315-323 (2014).

[42] Li L. H., Lu J., Wang Z. S., Yang L., Zhou X. F., Han L., Fabrication of the C-N Co-Doped Rod-Like TiO_2 Photocatalyst with Visible-Light Responsive Photocatalytic Activity, *Mater. Res. Bull.*, **47**(6): 1508-1512 (2012).

[43] Cheng X., Yu X., Xing Z., Synthesis and Characterization of C-N-S-tridoped TiO_2 Nano-Crystalline Photocatalyst and Its Photocatalytic Activity for Degradation of Rhodamine B, *J. Phy. Chem. Solids*, **74**(5): 684-690 (2013).

[44] Pang Y. L., Abdullah A. Z., Effect of Carbon and Nitrogen Co-Doping on Characteristics and Sonocatalytic Activity of TiO_2 Nanotubes Catalyst for Degradation of Rhodamine B in Water, *Chem. Eng. J.*, **214**: 129-138 (2013).

[45] Yu J.G., Yu H.G., Cheng B., Zhao X.J., Yu J.C., Ho W.K., The Effect of Calcination Temperature on the Surface Microstructure and Photocatalytic Activity of TiO_2 Thin Films Prepared by Liquid Phase Deposition, *J. Phys. Chem. B*, **107**(50): 13871–13879 (2003).

[46] Mani A. D., Kumar Reddy P. M., Srinivaas M., Ghosal P., Xanthopoulos N., Subrahmanyam C., Facile Synthesis of Efficient Visible Active C-Doped TiO_2 Nanomaterials with High Surface Area for the Simultaneous Removal of Phenol and Cr(VI), *Mater. Res. Bull.*, **61**: 391-399 (2015).

[47] Zhou P., Yu J., Wang Y., The New Understanding on Photocatalytic Mechanism of Visible-Light Response N-S Codoped Anatase TiO_2 by First-Principles, *Appl. Catal. B: Environ.*, **142-143**: 45-53 (2013).

[48] Kim N. J., La Y. H., Im S. H., Ryu B. K., Optical and Structural Properties of Fe-TiO_2 Thin Films Prepared by Sol-Gel Dip Coating, *Thin Solid Films*, **518**(24): 156-160 (2010).

[49] Talebian A., Entezari M. H., Ghows N., Complete Mineralization of Surfactant from Aqueous Solution by a Novel Sono-Synthesized Nanocomposite (TiO_2-Cu_2O) under Sunlight Irradiation, *Chem. Eng. J.*, **229**: 304-312 (2013).

[50] Reddy D. R., Kumaravel Dinesh G., Anandan S., Sivasankar T., Sonophotocatalytic Treatment of Naphtol Blue Black Dye and Real Textile Wastewater Using Synthesized Fe-Doped TiO_2, *Chem. Eng. Process: Process Intensification*, **99**: 10-18 (2016).

[51] He J., Gou R., Fang L., Dong W., Zheng F., Shen M., Characterization and Visible Light Photocatalytic Mechanism of Size-Controlled $BiFeO_3$ Nanoparticles, *Mater. Res. Bull.*, **48**(9): 3017-3024 (2013).

[52] Rodríguez E. M., Márquez G., Tena M., Álvarez P. M., Beltrán F. J., Determination of Main Species Involved in the First Steps of TiO_2 Photocatalytic Degradation of Organics with the Use of Scavengers: The Case of Ofloxacine, *Appl. Catal. B: Environ.*, **178**: 44-53 (2015).

[53] Zhou L., Song W., Chen Z., Yin G., Degradation of Organic Pollutants in Wastewater by Bicarbonate-Activated Hydrogen Peroxide with a Supported Cobalt Catalyst, *Environ. Sci. Technol.*, **47**(8): 3833-3839 (2013).

[54] Li F., Kang Y., Chen M., Liu G., Lv W., Yao K., Chen P., Huang H., Photocatalytic Degradation and Removal Mechanism of Ibuprofen via Monoclinic $BiVO_4$ under Simulated Solar Light, *Chemosphere*, **150**: 139-144 (2016).